The Fermi surface and the role of electronic correlations in $Sm_{2-x}Ce_xCuO_4$

2010 J. Phys.: Condens. Matter 22 015701

(http://iopscience.iop.org/0953-8984/22/1/015701)

J. Phys.: Condens. Matter **22** (2010) 015701 (6pp) doi:10.1088/0953-8984/22/1/015701

The Fermi surface and the role of electronic correlations in $Sm_{2-x}Ce_xCuO_4$

M M Korshunov[1,2,6], E V Zakharova[2], I A Nekrasov[3], Z V Pchelkina[4] and S G Ovchinnikov[2,5]

[1] Max-Planck-Institut für Physik komplexer Systeme, D-01187 Dresden, Germany
[2] L V Kirensky Institute of Physics, Siberian Branch of Russian Academy of Sciences, Krasnoyarsk 660036, Russia
[3] Institute for Electrophysics, Russian Academy of Sciences, Ekaterinburg 620016, Russia
[4] Institute for Metal Physics, Russian Academy of Sciences, Ekaterinburg 620219, Russia
[5] Siberian Federal University, Krasnoyarsk 660041, Russia

E-mail: korshunov@phys.ufl.edu

Received 4 September 2009, in final form 19 October 2009
Published 2 December 2009
Online at stacks.iop.org/JPhysCM/22/015701

Abstract

Using a LDA + GTB (local density approximation + generalized tight-binding) hybrid scheme we investigate the band structure of the electron-doped high-T_c material $Sm_{2-x}Ce_xCuO_4$. Parameters of the minimal tight-binding model for this system (the so-called three-band Emery model) were obtained within the NMTO (Nth-order muffin-tin orbital) method. The doping evolution of the dispersion and the Fermi surface in the presence of electronic correlations was investigated in two regimes of magnetic order: short-range (spin-liquid) and long-range (antiferromagnetic metal). Each regime is characterized by the specific topologies of the Fermi surfaces and we discuss their relation to recent experimental data.

(Some figures in this article are in colour only in the electronic version)

1. Introduction

One of the most important questions in condensed matter is how the strong interaction between quasiparticles modifies their properties and influences observable quantities. Non-Fermi-liquid behavior was found in many different substances, but a class of high-T_c copper oxides has attracted special attention during the last few decades. The unconventional, non-s-wave, superconductivity has a lot to do with it. While other players came to the stage, like lamellar sodium cobalt oxides and iron-based pnictide superconductors, only high-T_c cuprates combine both strong electronic correlations and high values of critical temperature.

A key issue in a theory of high-T_c superconductivity is the proper description of the low-energy electronic structure. Recent experimental results, mainly of angle-resolved photoemission spectroscopy (ARPES) [1–3] and measurements of quantum oscillations [4–6], provide a pattern to test various theoretical models and schemes. One of the approaches, proposed by some of the present authors, is the LDA + GTB hybrid scheme [7]. It was shown that the mean-field theory within this scheme captures the most essential features of the doping-dependent evolution of the quasiparticle band structure and the Fermi surface [8, 9].

A lot of theoretical and experimental efforts were concentrated on the hole-doped compounds. Systems with electron doping, $Re_{2-x}Ce_xCuO_4$ (Re = Nd, Pr and Sm), present a counterpart to hole-doped ones and a test for electron–hole asymmetry in Mott–Hubbard insulators. Recent ARPES data on the optimally doped, $x = 0.14$, Sm-based compound provide detailed information on the Fermi surface and the band dispersion in the vicinity of the Fermi level [10]. A similar study was reported for Nd-based compounds by Schmitt *et al* [11]. These results were confirmed independently by the measurement of the quantum oscillations [12]. Also, Park *et al* [10] presented an explanation of the observed data based on the $\sqrt{2} \times \sqrt{2}$ spin-density wave (SDW) model. On the other hand, the high-energy electronic structure is found to be inconsistent with the SDW scenario. Moreover, the SDW model implies weak or moderate electronic correlations and a Fermi liquid background, which is obviously not the case for the underdoped and optimally doped cuprates. Thus it is not

[6] Present address: Department of Physics, University of Florida, Gainesville, FL 32611, USA.

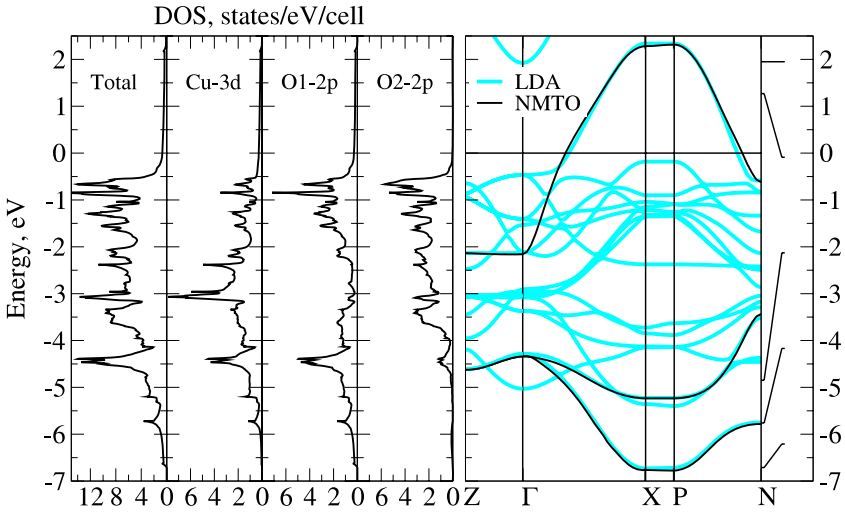

Figure 1. The electronic structure of Sm_2CuO_4 obtained within LDA. The left panel presents the total and partial densities of states; the right panel shows band dispersions: thick (cyan) curves denote LMTO bands, while thin (black) curves denote NMTO bands. Zero corresponds to the Fermi level.

a satisfactory scenario and strong correlation effects should be taken into account.

Here we present the investigation of the electronic structure for the electron-doped high-T_c material $Sm_{2-x}Ce_xCuO_4$ by means of the LDA + GTB hybrid scheme. Parameters of a minimal generic tight-binding model for these systems (the so-called Emery model) were obtained within the NMTO method. The doping evolution of the band structure and the Fermi surface within this model, in the presence of strong electronic correlations and magnetic fluctuations, was studied in the framework of the GTB method.

The LDA + GTB electronic structure strongly depends on the underlying magnetic order. Although there is no Néel temperature in the optimally doped n-type cuprates, the antiferromagnetic (AFM) correlation length is extremely large ($\lambda \approx 400a$) up to $x = 0.17$ [13–16]. Such a correlation length causes the magnetic behavior to be rather close to the long-range ordered AFM. That is why our spin-liquid description is unable to capture some details of the observed Fermi surface. On the other hand, there is good agreement with the recent ARPES data once we assume the presence of the long-range order.

2. The noninteracting band structure

Here we will describe the noninteracting band structure and in the next section introduce the electronic correlations within the LDA + GTB method.

The Sm_2CuO_4 system has a body-centered tetragonal crystal structure with the space group $I4/mmm$. Values of lattice parameters are $a = 3.917$ Å and $c = 11.899$ Å. The atomic positions for different atoms are: Cu (0, 0, 0), Sm (0, 0, 0.351 84) and two types of oxygens O1 (0, 0.5, 0) and O2 (0, 0.5, 0.25) [17]. Physically important CuO_2 layers are constructed with O1 type oxygens. No apical oxygen is present in this structure.

We perform density functional theory band structure calculations within the linear muffin-tin orbital basis set employing an atomic sphere approximation in the framework of the program package TB-LMTO-ASA v47 [18–20]. In figure 1 results of our LMTO computations are presented. The left panel shows the total and the partial densities of states. Cu-3d and O1-2p states cross the Fermi level. In the right panel of figure 1 LMTO band dispersions are presented (thick curves). Note the Fermi level is crossed by just one antibonding hybrid Cu-3d–O1-2p band of x^2–y^2 symmetry. It is in agreement with the generic minimal tight-binding model for high-T_c cuprates [21, 22]. The orbital basis for this model consists of a Cu-3$d_{x^2-y^2}$ orbital and in-plane p_x and p_y oxygen orbitals. To compute the corresponding model parameters the Nth-order muffin-tin orbital method (NMTO) [23] was used. Necessary NMTO expansion energies are schematically shown on the right side of figure 1. The obtained hopping parameters are listed in table 1, and the single-electron energies are $E_{x^2-y^2} = -2.322$ eV and $E_{p_x} = -3.708$ eV.

We assume that the values of Coulomb repulsion U and Hund's exchange J_H for Cu ions are doping-independent and equal to 10 eV and 1 eV, respectively (see [7] for details).

Table 1. Parameters for the three-band model obtained within the NMTO method. Here x^2 and $p_{x,y}$ denote the Cu-3$d_{x^2-y^2}$ and O-$p_{x,y}$ orbital indexes. All values are in eV.

	Involved orbitals					
	(x^2, p_x)		(x^2, x^2)		(p_x, p_y)	
Hopping	Direction	Value	Direction	Value	Direction	Value
t	(0.5, 0)	1.261	(1, 0)	0.138	(0.5, 0.5)	0.882
t'	(0.5, 1)	−0.011	(1, 1)	−0.025	(1.5, 0.5)	0.033
t''	(1.5, 0)	0.1	(2, 0)	0.011	(1.5, 1.5)	0.021
t'''	(1.5, 1)	−0.007	(1, 2)	−0.012	(2.5, 0.5)	0.005

3. LDA + GTB scheme

Within the LDA + GTB method [7] the results of *ab initio* band structure calculations presented in the previous section

are used to construct the Wannier functions and to obtain the parameters of the multiband Hubbard-type model. For this multiband model the electronic structure in the strong correlation regime is calculated within the generalized tight-binding (GTB) method [24–26]. The latter combines the exact diagonalization of the model Hamiltonian for a small cluster (unit cell) with perturbative treatment of the intercluster hopping and interactions. After this step we end up with the GTB Hamiltonian. Depending on the order of perturbative treatment, we can formulate different approximations.

As was shown before [7], for undoped and weakly doped $La_{2-x}Sr_xCuO_4$ and $Nd_{2-x}Ce_xCuO_4$ this scheme in the lowest order in hopping (Hubbard-I approximation) results in a charge-transfer insulator with a correct value of the gap E_{ct} and the dispersion of bands in agreement with the experimental ARPES data.

We map the GTB Hamiltonian onto the effective t–t'–t''–J^* model, where '$*$' denotes the three-site correlated hoppings, and we study two regimes of AFM correlations. Namely, the spin-liquid phase with short-range AFM fluctuations and the long-range AFM metallic phase. We will describe the AFM metallic phase using the Hubbard-I approximation that was shown to be in qualitative agreement with the quantum Monte Carlo results [27]. To study the spin-liquid phase, we use the same procedure as in [8] and go beyond the Hubbard-I approximation: (i) we solve the Dyson equation in the paramagnetic phase by means of the diagram technique for the Hubbard X operators [28], (ii) obtain the coupled equations for the self-energy $\hat{\Sigma}(\mathbf{k},\omega)$, the strength operator $\hat{P}(\mathbf{k},\omega)$, and the spin–spin and kinematic correlation functions and (iii) we solve the coupled equations self-consistently and obtain a doping-dependent Fermi surface and the band structure.

The t–t'–t''–J^* model Hamiltonian is given by

$$H_{t-J^*} = H_{t-J} + H_{(3)},$$

$$H_{t-J} = \sum_{f,\sigma}(\varepsilon-\mu)X_f^{\sigma\sigma} + \sum_{f\neq g,\sigma} t_{fg}X_f^{\sigma 0}X_g^{0\sigma} + \sum_{f\neq g} J_{fg}(\mathbf{S}_f\cdot\mathbf{S}_g - \tfrac{1}{4}n_f n_g) \quad (1)$$

$$H_{(3)} = \sum_{f\neq m\neq g,\sigma} \frac{\tilde{t}_{fm}\tilde{t}_{mg}}{U}(X_f^{\sigma 0}X_m^{\bar{\sigma}\sigma}X_g^{0\bar{\sigma}} - X_f^{\sigma 0}X_m^{\bar{\sigma}\bar{\sigma}}X_g^{0\sigma}),$$

where $X_f^{nn'} \equiv |n\rangle\langle n'|$ are the Hubbard X operators [29] acting on the Hilbert space of local states $|n\rangle = \{0,\sigma,-\sigma \equiv \bar{\sigma}\}$, $J_{fg} = 2\tilde{t}_{fg}^2/U$ is the AFM exchange between two sites f and g, $U = E_{ct}$ is the effective Hubbard repulsion determined by the charge-transfer energy $E_{ct} \approx 2$ eV, $t_{\mathbf{k}} = 2t(\cos k_x + \cos k_y) + 4t'\cos k_x \cos k_y + 2t''(\cos 2k_x + \cos 2k_y)$ is the Fourier transform of the hopping t_{fg}, and $\tilde{t}_{\mathbf{k}} = 2\tilde{t}(\cos k_x + \cos k_y) + 4\tilde{t}'\cos k_x \cos k_y + 2\tilde{t}''(\cos 2k_x + \cos 2k_y)$ is the Fourier transform of the interband hopping parameter $\tilde{t}_{fg}$, $\mathbf{S}_f$ is the spin operator, ε is the one-hole local energy and μ is the chemical potential. The Green function in terms of the Hubbard X operators is

$$G_\sigma(\mathbf{k},\omega) = \left\langle\!\left\langle X_{\mathbf{k}}^{0\sigma} \middle| X_{\mathbf{k}}^{\sigma 0}\right\rangle\!\right\rangle_\omega = \frac{(1+x)/2}{\omega - \varepsilon_0 + \mu - \frac{1+x}{2}t_{\mathbf{k}} - \frac{1-x^2}{4}\frac{\tilde{t}_{\mathbf{k}}^2}{U} - \Sigma(\mathbf{k})}. \quad (2)$$

Within our approximations [8], the strength operator $\hat{P}(\vec{k},E)$ is replaced by the occupation factor $(1+x)/2$ and the self-energy $\hat{\Sigma}(\mathbf{k},\omega)$ is frequency-independent but preserves momentum dependence:

$$\Sigma(\mathbf{k}) = \frac{2}{1+x}\frac{1}{N} \times \sum_{\mathbf{q}}\left\{\left[t_{\mathbf{q}} - \frac{1-x}{2}J_{\mathbf{k}-\mathbf{q}} - x\frac{\tilde{t}_{\mathbf{q}}^2}{U} - (1+x)\frac{\tilde{t}_{\mathbf{k}}\tilde{t}_{\mathbf{q}}}{U}\right]K_{\mathbf{q}} + \left[t_{\mathbf{k}-\mathbf{q}} - \frac{1-x}{2}\left(J_{\mathbf{q}} - \frac{\tilde{t}_{\mathbf{k}-\mathbf{q}}^2}{U}\right) - (1+x)\frac{\tilde{t}_{\mathbf{k}}\tilde{t}_{\mathbf{k}-\mathbf{q}}}{U}\right]\cdot\frac{3}{2}C_{\mathbf{q}}\right\}. \quad (3)$$

The spin–spin $C_{\mathbf{q}}$ and kinematic $K_{\mathbf{q}}$ correlation functions play a significant role representing the short-range AFM fluctuations and the kinetic energy reduced by the correlation effects, respectively

$$C_{\mathbf{q}} = \sum_{\mathbf{f}-\mathbf{g}} e^{-i(\mathbf{f}-\mathbf{g})\mathbf{q}}\left\langle X_{\mathbf{f}}^{\sigma\bar{\sigma}}X_{\mathbf{g}}^{\bar{\sigma}\sigma}\right\rangle = 2\sum_{\mathbf{f}-\mathbf{g}} e^{-i(\mathbf{f}-\mathbf{g})\mathbf{q}}\left\langle S_{\mathbf{f}}^z S_{\mathbf{g}}^z\right\rangle,$$
$$K_{\mathbf{q}} = \sum_{\mathbf{f}-\mathbf{g}} e^{-i(\mathbf{f}-\mathbf{g})\mathbf{q}}\left\langle X_{\mathbf{f}}^{\sigma 0}X_{\mathbf{g}}^{0\sigma}\right\rangle. \quad (4)$$

The energy spectrum is determined by the poles of the Green function (2) and the Fermi surface is determined by the equation $\varepsilon_0 - \mu + \frac{1+x}{2}t_{\mathbf{k}} + \frac{1-x^2}{4}\frac{\tilde{t}_{\mathbf{k}}^2}{U} + \Sigma(\mathbf{k}) = 0$.

4. Results and discussion

The procedure of mapping the GTB Hamiltonian onto the effective model was described in detail in [7]. Following the same steps and using the parameters listed in table 1, we obtain the t–t'–t''–J^* model with the following hoppings and exchange interactions: $t = -0.59$ eV, $t' = -0.08t$, $t'' = 0.15t$, $J = 0.92|t|$, $J' = 0.01|t|$, $J'' = 0.02|t|$, $\tilde{t} = -0.74$ eV, $\tilde{t}' = -0.11\tilde{t}$ and $\tilde{t}'' = 0.16\tilde{t}$. Here, $\tilde{t}$, $\tilde{t}'$, and $\tilde{t}''$ are the interband hoppings through the charge-transfer gap, which determine the three-site hoppings and the exchange parameter, $J = 2\tilde{t}^2/E_{ct}$. Note that, although the value of the nearest-neighbor exchange J is quite large, the spin gap in the AFM phase will be determined not by this value alone. There will also be a contribution from the three-site hoppings. This contribution reduces the value of the spin gap, as will be discussed later.

In figure 2 we present results for the t–t'–t''–J^* model in the spin-liquid phase. At low doping, $x = 0.03$, due to the scattering on the magnetic fluctuations, the band structure possess local AFM symmetry in the vicinity of the $(\pm\pi/2,\pm\pi/2)$ points (see figure 2(a)) and the Fermi surface has a form of four electron pockets around the $(0,\pm\pi)$ and $(\pm\pi,0)$ points. Values of the spin–spin correlation functions $C_{\mathbf{q}}$ are large enough for the similar topology to survive until $x \approx 0.22$, where a quantum phase transition with a change of the Fermi surface topology takes place. After the transition, the Fermi surface at $x = 0.22$ has the form of a large hole pocket around the (π,π) point and a small hole pocket around the $(0,0)$ point, which decrease in size with further electron doping. At $x = 0.25$ only one large hole pocket

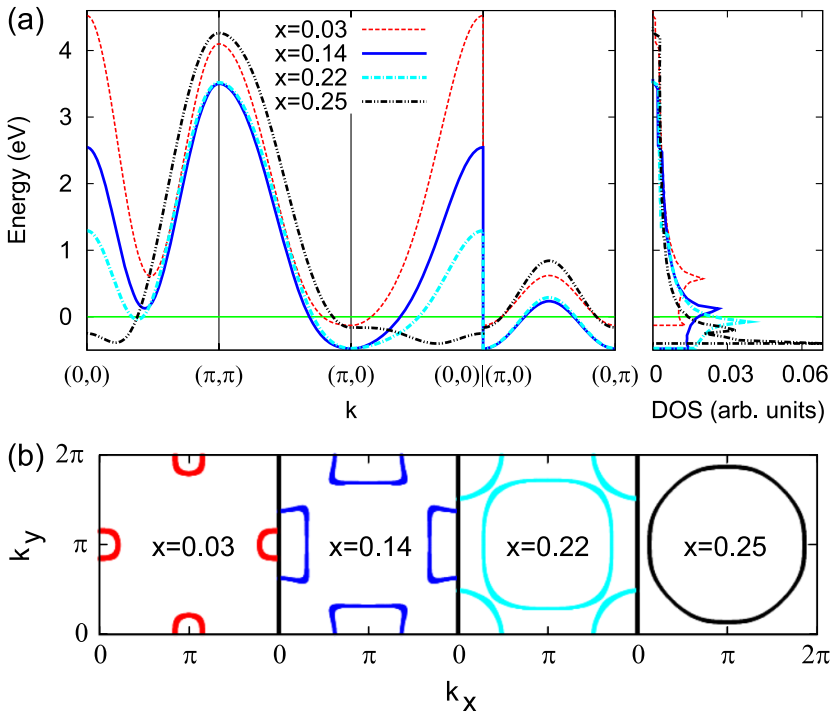

Figure 2. Spin-liquid phase: band structure and DOS (a) and the Fermi surface (b) for $Sm_{2-x}Ce_xCuO_4$ within the LDA + GTB method for different doping concentrations x, as indicated. In (a) zero corresponds to the Fermi level.

around the (π, π) point is left. The quantum phase transition with the change of the Fermi surface topology was found experimentally in an Nd-based compound [12], though at a different critical concentration.

Note that the standard formulation of the Luttinger theorem does not work for the Hubbard fermions since the spectral weight of such fermions is determined by the strength operator, $\hat{P}(\mathbf{k}, E) = F_{0\sigma}$, and each quantum state contains $2F_{0\sigma} = 1 - x$ electrons. A generalized Luttinger theorem for the strongly correlated systems [32] takes into account the spectral weight of each $|k\rangle$ state and the Fermi surface in our figure 2 satisfies its completely.

A comparison of the calculated Fermi surface in the spin-liquid phase and the experimental ARPES data [10] is shown in figure 3. Note the difference in the methods to obtain the Fermi surface 'mapping'. We draw a set of constant energy cuts from the Fermi level down to −0.3 eV below it, while the experimental Fermi surface mapping is an integration of ARPES intensities over the 30 meV energy window. The ARPES Fermi surface consists of three parts: two pockets around the $(0, \pi)$ and $(\pi, 0)$ points, and one elongated pocket around the $(\pi/2, \pi/2)$ point. One can immediately notice from figure 2(b) that in our spin-liquid theory the pocket around the $(\pi/2, \pi/2)$ point is missing; it does not appear even if one collects intensities from below the Fermi level, as seen in figure 3. Moreover, there are no features in the band dispersion, which could produce such a pocket. Thus we conclude that our theory for the spin-liquid phase does not reproduce all details of the experimental Fermi surface.

Since optimally doped $Sm_{2-x}Ce_xCuO_4$ is in the vicinity of the ordered AFM phase and the correlation length is extremely

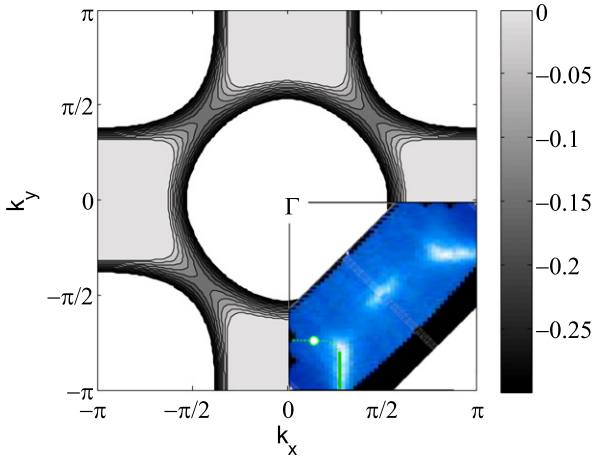

Figure 3. Fermi surface 'mapping' (set of equipotential cuts from the Fermi level to −0.3 eV below it) in the spin-liquid phase for $x = 0.14$ together with the reproduction of experimental ARPES data from [10] in the lower right corner. The color bar on the right shows the correspondence between shades of gray and energy from the Fermi level (in eV).

large (about 400 lattice constants) [16], we now investigate the band structure in the t–t'–t''–J^* model assuming the long-range AFM order. The procedure is similar to [30, 31], where the energy spectrum of the t–t'–t''–J model was obtained within the Hubbard-I approximation, but here we also take the three-site hopping terms into account.

In figure 4(b) we present results for the Fermi surface in the AFM phase of the t–t'–t''–J^* model at $x = 0.14$

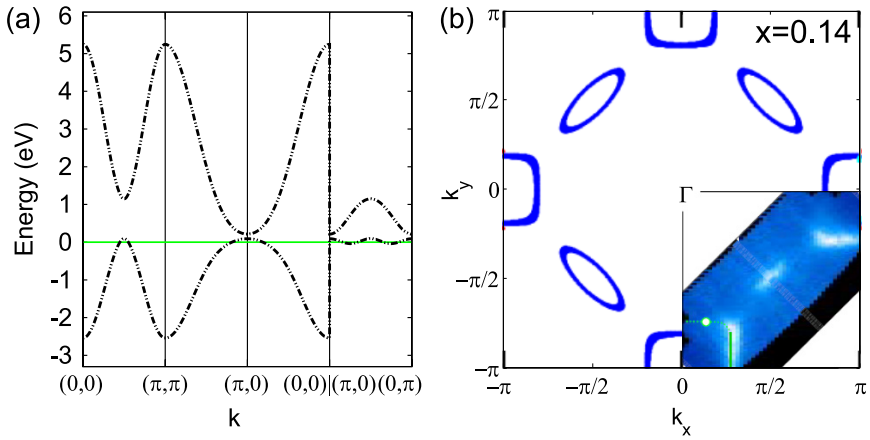

Figure 4. AFM phase: band structure (a) and the Fermi surface (b) for $x = 0.14$ within the LDA + GTB method. In the lower right corner of (b) we show the reproduction of the ARPES Fermi surface map from [10]. In (a) zero corresponds to the Fermi level.

together with the experimental ARPES data. Evidently, there is rather good agreement between both. We would like to mention that for lower concentrations our calculations result in a decrease of pockets around the $(\pi/2, \pi/2)$ points and an increase of pockets around the $(\pi, 0)$ and $(0, \pi)$ points. Note that in the t–J model the spin gap is determined solely by the AFM exchange J [30]. Here, momentum dependence of the spin gap is proportional to $t' \cos k_x \cos k_y$ (see equation (12) of [30]). The reason is that, in the absence of spin fluctuations, the hopping of a particle without spin flip processes is possible only within the same spin sublattice. Because of the $\cos k_x \cos k_y$ functional form the spin gap is maximal at the $(\pi/2, \pi/2)$ point and minimal at the $(\pi, 0)$ point as seen in figure 4(a). Since the three-site hopping terms involving sites f, m, and g are proportional to $\tilde{t}_{fm}\tilde{t}_{mg}/E_{\rm ct}$, they also contribute to the spin gap; but, apparently, they decrease the gap value around the $(\pi, 0)$ point, making it more anisotropic.

Since we are making a mean-field theory (though in a strong interaction limit) we cannot address the question of the intensity distribution over the Fermi surface. This question was addressed earlier by different groups [33, 34]. Remarkably, their results on the Fermi surface contours for $x \approx 0.14$ are very similar to ours in figure 4 in spite of rather different calculation schemes. This again emphasizes the fact that the AFM correlations are very strong in the optimally electron-doped cuprates and they determine the quasiparticle dispersion and the Fermi surface.

5. Conclusion

We have shown that the experimentally observed Fermi surface topology can be explained within the LDA + GTB calculations for the long-range AFM spin background. On the other hand, our theory for the spin-liquid phase demonstrates only partial agreement with the ARPES Fermi surface due to the underestimation of the impact of magnetic scattering on the electronic structure. We conclude that the spin fluctuations are very strong in $Sm_{1.86}Ce_{0.14}CuO_4$ and are closer to the long-range AFM fluctuations rather than to the fluctuations in the spin-liquid phase. A similar conclusion was drawn recently from the analysis of quantum oscillations in Nd-based electron-doped cuprates [12].

We would like to emphasize the significant difference between our picture for AFM order and one by Park *et al* [10]. Park *et al* provide a simple calculation based on the conventional SDW order i.e. the one based on a weak coupling approximation for the interaction. In the absence of long-range order the ground state is metallic even at zero doping, $x = 0$. On the other hand, our approach allows us to study the limit of large interaction and provides an insulating ground state at zero doping. This is an essential difference since the underdoped cuprates belong to a class of strongly interacting systems and exhibit a Mott transition at a half-filling, $x = 0$. More precisely, because of the copper–oxygen hybridization the cuprates show the charge-transfer gap $E_{\rm ct}$ at $x = 0$, but on the level of a single-band Hubbard model one can speak about a Mott–Hubbard effective gap $U = E_{\rm ct}$.

Acknowledgments

We would like to thank A A Kordyuk and I Eremin for useful discussions. The authors acknowledge support from RFBR (grants 08-02-00021, 10-02-00662, 08-02-91200 and 07-02-00226), the RAS programs on 'Low temperature quantum phenomena', 'Quantum physics of condensed matter' and 'Strongly correlated electrons solids', President of Russia (grants MK-614.2009.2 (IN) and MK-3227.2008.2 (ZP)), Scientific School (grant SS-1929.2008.2), Interdisciplinary UB-SB RAS project, Dynasty Foundation (ZP) and Russian Science Support Foundation (IN).

References

[1] Yoshida T, Zhou X J, Sasagawa T, Yang W L, Bogdanov P V, Lanzara A, Hussain Z, Mizokawa T, Fujimori A, Eisaki H, Shen Z-X, Kakeshita T and Uchida S 2003 *Phys. Rev. Lett.* **91** 027001

[2] Damascelli A, Hussain Z and Shen Z-X 2003 *Rev. Mod. Phys.* **75** 473

[3] Meng J, Liu G, Zhang W, Zhao L, Liu H, Jia X, Mu D, Liu S, Dong X, Lu W, Wang G, Zhou Y, Zhu Y, Wang X, Xu Z, Chen C and Zhou X J 2009 *Nature* **462** 335
[4] Doiron-Leyraud N, Proust C, LeBoeuf D, Levallois J, Bonnemaison J-B, Liang R, Bonn D A, Hardy W N and Taillefer L 2007 *Nature* **447** 565
[5] Yelland E A, Singleton J, Mielke C H, Harrison N, Balakirev F F, Dabrowski B and Cooper J R 2008 *Phys. Rev. Lett.* **100** 047003
[6] Sebastian S E, Harrison N, Palm E, Murphy T P, Mielke C H, Liang R, Bonn D A, Hardy W N and Lonzarich G G 2008 *Nature* **454** 200
[7] Korshunov M M, Gavrichkov V A, Ovchinnikov S G, Nekrasov I A, Pchelkina Z V and Anisimov V I 2005 *Phys. Rev.* B **72** 165104
[8] Korshunov M M and Ovchinnikov S G 2007 *Eur. Phys. J.* B **57** 271
[9] Korshunov M M, Gavrichkov V A, Ovchinnikov S G, Nekrasov I A, Kokorina E E and Pchelkina Z V 2007 *J. Phys.: Condens. Matter* **19** 486203
[10] Park S R, Roh Y S, Yoon Y K, Leem C S, Kim J H, Kim B J, Koh H, Eisaki H, Armitage N P and Kim C 2007 *Phys. Rev.* B **75** 060501(R)
[11] Schmitt F, Lee W S, Lu D-H, Meevasana W, Motoyama E, Greven M and Shen Z-X 2008 *Phys. Rev.* B **78** 100505(R)
[12] Helm T, Kartsovnik M V, Bartkowiak M, Bittner N, Lambacher M, Erb A, Wosnitza J and Gross R 2009 *Phys. Rev. Lett.* **103** 157002
[13] Sumarlin I W, Skanthakumar S, Lynn J W, Peng J L, Li Z Y, Jiang W and Greene R L 1992 *Phys. Rev. Lett.* **68** 2228
[14] Gukasov A G, Polyakov V A, Zobkalo I A, Petitgrand D, Bourges P, Boudaréne L, Barilo S N and Zhigunov D N 1995 *Solid State. Commun.* **95** 533
[15] Chang B C, Hsu Y Y and Ku H C 2002 *Physica* B **312/313** 59
[16] Motoyama E M, Yu G, Vishik I M, Vajk O P, Mang P K and Greven M 2007 *Nature* **445** 186
[17] Takeda H, Okuno M, Ohgaki M, Yamashita K and Matsumoto T 2000 *J. Mater. Res.* **15** 1905
[18] Andersen O K 1975 *Phys. Rev.* B **12** 3060
[19] Gunnarsson O, Jepsen O and Andersen O K 1983 *Phys. Rev.* B **27** 7144
[20] Andersen O K and Jepsen O 1984 *Phys. Rev. Lett.* **53** 2571
[21] Emery V J 1987 *Phys. Rev. Lett.* **58** 2794
[22] Varma C M, Schmitt-Rink S and Abrahams E 1987 *Solid State Commun.* **62** 681
[23] Andersen O K and Saha-Dasgupta T 2000 *Phys. Rev.* B **62** 16219(R)
[24] Ovchinnikov S G and Sandalov I S 1989 *Physica* C **161** 607
[25] Gavrichkov V A, Ovchinnikov S G, Borisov A A and Goryachev E G 2000 *Zh. Eksp. Teor. Fiz.* **118** 422
Gavrichkov V A, Ovchinnikov S G, Borisov A A and Goryachev E G 2000 *JETP* **91** 369 (Engl. Transl.)
[26] Gavrichkov V A, Borisov A A and Ovchinnikov S G 2001 *Phys. Rev.* B **64** 235124
[27] Ovchinnikov S G and Shneyder E I 2003 *Central Eur. J. Phys.* **3** 421
[28] Ovchinnikov S G and Val'kov V V 2004 *Hubbard Operators in the Theory of Strongly Correlated Electrons* (London: Imperial College Press)
[29] Hubbard J C 1964 *Proc. R. Soc.* A **277** 237
[30] Ovchinnikov S G, Borisov A A, Gavrichkov V A and Korshunov M M 2004 *J. Phys.: Condens. Matter* **16** L93
[31] Ovchinnikov S G, Korshunov M M and Zakharova E V 2008 *Fiz. Tverd. Tela* **50** 1349
Ovchinnikov S G, Korshunov M M and Zakharova E V 2008 *Phys. Solid State* **50** 1401 (Engl. Transl.)
[32] Korshunov M M and Ovchinnikov S G 2003 *Fiz. Tverd. Tela* **45** 1351
Korshunov M M and Ovchinnikov S G 2003 *Phys. Solid State* **45** 1415 (Engl. Transl.)
[33] Aichhorn M, Arrigoni E, Potthoff M and Hanke W 2006 *Phys. Rev.* B **74** 024508
[34] Kokorina E E, Kuchinskii E Z, Nekrasov I A, Pchelkina Z V, Sadovskii M V, Sekiyama A, Suga S and Tsunekawa M 2008 *JETP* **107** 828